Proceedings of the ASME 2013 Dynamic Systems and Control Conference
DSCC2013
October 21-23, 2013, Palo Alto, California, USA

DSCC2013-4007

STRUCTURAL DYNAMIC IMAGING THROUGH INTERFACES USING PIEZOELECTRIC ACTUATION AND LASER VIBROMETRY FOR DIAGNOSING THE MECHANICAL PROPERTIES OF COMPOSITE MATERIALS

Christopher C. Watson, Jeffrey F. Rhoads, and Douglas E. Adams
School of Mechanical Engineering
Purdue University
West Lafayette, IN 47906
Email: deadams@purdue.edu

ABSTRACT

In many engineering applications, diagnostic techniques are needed to characterize the mechanical properties of internal components that are not readily visible at the surface of an object, as in the use of nondestructive testing to detect sub-surface damage in composite materials. Understanding the role of structural interfaces between two bodies is a key factor in developing these diagnostic techniques because the mechanical and geometric properties of the interface determine the degree to which measurements on the surface can be used to interrogate sub-surface components. In this paper, vibration measurements on a polycarbonate material, henceforth referred to as the buffer, are used to characterize the mechanical properties of a polymer particulate composite, henceforth referred to as the target, which is located beneath the buffer. To this end, a three-dimensional laser Doppler vibrometer and piezoelectric inertial actuator are used to measure the broadband response of the two-body structural dynamic system. Because of the importance of the actuator dynamics to the diagnostic measurements, a descriptive model is developed to better understand these dynamics and interpret the results. The longitudinal dynamics of the two-body system are shown to involve stronger coupling between the target and buffer materials as compared to the transverse dynamics. A Complex Mode Indicator Function is then used to extract the modal deflection shapes, and it is shown that the interface between the bodies introduces complexity in the dynamic response. Changes in the surface velocity of the buffer material are also studied as a function of a key mechanical property - the volume fraction of crystals in the target composite material. It is demonstrated that both the linear and nonlinear vibration characteristics of the buffer material change as a function of the composition of the target material, suggesting that a compositional diagnostic procedure is possible using surface vibration measurements.

INTRODUCTION

Imaging techniques are regularly employed in medical and security settings, amongst others, to illuminate anomalies in materials using x-ray, ultrasonic, thermographic, and other kinds of measurement systems. One example of this in engineering contexts is in nondestructive evaluation wherein nondestructive measurements are commonly used to inspect composite materials for sub-surface defects, such as face sheet delamination in sandwich composite materials. Here, the interlaminar crack can be detected using measurements that are performed on the surface of the material. In many cases, however, this type of material damage is difficult to ascertain due to the influence of complex structural interfaces between the measured surface and the material to be inspected. For example, it is difficult to detect damage in the solid propellant of a rocket motor, as it is located beneath a liner, which forms an interface with the propellant. Accordingly, measurements used to inspect the propellant must be capable of penetrating the liner, and data analysis techniques which take into account the effects of the interface must be developed.

In this paper, the imaging application of interest is the characterization of a particulate composite material, consisting of ammonium chloride crystals embedded in a hydroxyl-terminated polybutadiene (HTPB) polymer matrix. This composite is examined in two different crystal to polymer

volume fraction (vf) configurations, 50% and 75%, which serve as inert surrogates for explosive materials. This surrogate is located beneath the surface of a polycarbonate buffer material, as shown in Figure 1. The specific objective of this study is to characterize the structural dynamic properties of the composite material beneath the buffer material using only non-contact surface measurements on the buffer material. A piezoelectric actuator is used to provide a periodic excitation to the buffer material and measurements taken on the buffer, as well as the composite material, with a Polytec three-dimensional laser Doppler vibrometer are used to characterize the structural dynamic response of the coupled system.

The structural interface between these two components is highlighted in Figure 1. This interface consists of a layer of vacuum grease between the buffer and the target. This interface was selected because it largely avoids the presence of air gaps, which introduce effects that are not examined within. The stiffness and damping properties of this interface affect the degree to which the applied force from the actuator excites the composite material. The interface also affects the degree to which the measurements on the buffer material reflect the behavior of the composite material beneath the interface. Using linear and nonlinear vibration experiments, together with simple vibration models, this paper develops a means for structural dynamic imaging of the internal composite material using measurements that are acquired solely from the surface of the external buffer material.

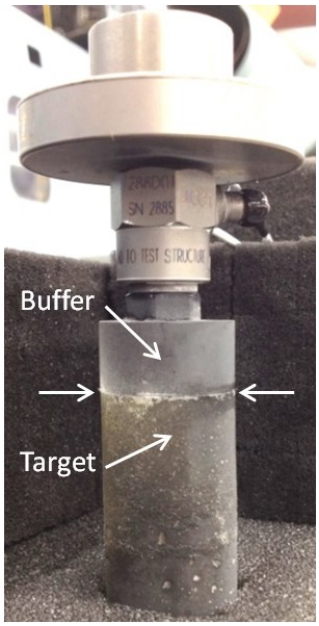

FIGURE 1: TEST SPECIMEN CONSISTING OF A CYLINDER OF PARTICULATE COMPOSITE MATERIAL (TARGET) BENEATH A CYLINDER OF POLYCARBONATE (BUFFER) TO WHICH AN INERTIAL PIEZOELECTRIC ACTUATOR IS ATTACHED.

PRIOR RELATED WORK

Before proceeding, it is prudent to review key prior work related to non-contact testing, structural interfaces, crystalline-based polymers, and the closely-related research area of structural damage detection.

From a general perspective, Doebling, Farrar, and Prime (1998) provide an overview of the general field of damage detection in mechanical and structural systems. They confine themselves to methods utilizing vibration response data. The underlying theory behind these methods is that physical properties such as mass, stiffness, and damping, are directly tied to modal parameters, such as mode shapes, resonant frequencies, and modal damping parameters. Damage to a physical system that will affect one or more of these physical properties will cause changes to the modal parameters. Similarly, Montalvao, Maia, and Ribeiro (2006) provide a review of vibration-based structural health monitoring referring to more than 200 published works, with a special emphasis paid to methods using composite materials and structures as case studies.

From a more focused perspective, Cerniglia, Djordjevic, and Nigrelli (2001) explore the use of non-contact nondestructive testing (NDT) to detect sub-surface defects in a thick composite test sample, thus negating the need for a couplant.

The two primary methods of non-contact NDT are thermal tomography, which is a widely used technique for characterizing damage in composite materials, and laser Doppler vibrometry (LDV). Castellini and Revel (2000) investigate the efficacy of LDV when compared with thermal tomography, finding that the measurement results correlated positively with defect attributes particular to composite materials, such as delamination extension, depth, and location. This indicates that LDV is well suited for characterizing damage in composite materials.

Moving on to interfaces and defects, Adams and Drinkwater (1997) explore the basic defects that can occur in a simple adhesive joint, and how NDT may or may not be suitable as a means of defect identification. There are several different types of defects that can occur in a simple adhesive joint. Poor adhesive strength, which is generally a function of poor surface preparation, is difficult to measure nondestructively. Other defects, such as voids, disbands, and porosity, which can result from improper manufacture, are more easily identified using NDT.

Bigoni and Movchan (2002) discuss the concept of a structural interface of finite width and joining continuous media. Their model differs from previous models in that they attribute a thickness to the structural interface, where others assume a zero thickness at the interface. With finite thickness comes inertia, which is consequential in the static problem, adding a structural parameter, as well as in the dynamic

problem, where the evaluation of transport properties of elastic structures is affected.

Bigoni, along with Bertoldi and Drugan (2006) seek to improve upon previous models of structural interfaces by introducing true structure, with geometrical and material properties, in the transition zone joining continuous bodies. Several cases are analytically solved, with the interesting result that the conventional zero-thickness linear interface model is represented as a special case of their structural continuum model.

Moving next to a review of particular methods used to excite materials with the goal of gaining information on the nature of the underlying interfaces, Donskoy and Sutin (2001) explore the use of modulated high and low frequency acoustic waves to exploit the nonlinearities created by weakly or incompletely bonded interfaces. The low frequency (LF) waves cause the interface to vary in contact area which causes the modulation of the phase and amplitude of the accompanying higher frequency (HF) waves. This creates side-band spectral components to the original HF signal in the frequency domain that can be considered as a new signal, the presence of which indicates a defect.

Guo, Zhang, and Wu (2010) attempt to evaluate the interfacial stiffness of contacting interfaces with a dual-frequency ultrasonic technique. Several types of interfaces are evaluated, and the linear and nonlinear interfacial stiffness is measured using a laser interferometer. The generated nonlinearities were found to decrease with increasing stiffness of contact, and the most problematic source of added nonlinearity was found to be at the interface between the transducer and the sample.

Finally, Mang, Hjelm, Skidmore, and Howe (1996) attempt to identify a means to quantitatively differentiate among the different defect types closely associated with high explosives which are composites of crystalline high explosives (HE) with binder materials. This relates to the motivation behind the research from which this paper emanates, and speaks to how the composition of the target material, and its defects, may or may not affect the properties of the interface between the buffer and target. Note that the defects can be due to naturally occurring density fluctuations, cracks in the HE and/or binder, voids, or other preparation related anomalies.

ACTUATOR DYNAMICS

In general, it is important to be cognizant of the fact that the dynamics of a system can be strongly influenced by the actuation and measurement systems used to characterize the system's response. Using a non-contact measurement helps alleviate concerns on the observation end, but the same cannot be said about the actuator utilized in this work, given its size relative to the sample being tested. In fact, actuator dynamics are particularly pertinent to this study because the actuator serves as the excitation source, participates in the modal response of the specimen, and strongly influences the level of excitation that is delivered to the buffer material in a frequency-dependent fashion. Accordingly, any conclusions that are made regarding changes in the measured response of the buffer and target materials, due to changes in the interface or the target material properties, should recognize the meaningful contributions of the dynamic response of the actuator.

To this end, the actuator assembly comprised of the actuator, proof mass, and impedance head (pictured in Figure 1) was investigated when it was being used to test the isolated polycarbonate specimen (buffer only), the isolated surrogate material (target only), and the combination of the two materials (as shown in Figure 2). By testing each of these configurations, the objective was to ascertain the common characteristics associated with the actuator dynamics, as well as the interface between the buffer and target materials. A PCB 712A02 actuator was used to provide the excitation using a 15V sine sweep drive signal with a burst chirp in the frequency range from 50-20,000 Hz. A Polytec PSV-400-3D scanning vibrometer was used to acquire response data on the specimens. The sample frequency was 51.2 kHz and the sample time was 640 msec. A PCB 288D01 impedance head was used to record the force and acceleration on the surface of the polycarbonate buffer material.

Figure 3(a) shows the averaged measured force spectra obtained from the impedance head across 10 measurements for each of the three configurations in Figure 2. The magnitude of the measured force is larger in the frequency range from 50-500 Hz, when the actuator reacts against the more massive surrogate material in the second two test configurations. The two resonances in this frequency range shift to lower frequencies in these two configurations due to the more massive surrogate material. In contrast, the antiresonance at approximately 930 Hz is roughly the same for all three configurations, suggesting that the antiresonance is primarily associated with the actuator assembly. This antiresonance corresponds to the situation where the force delivered at the impedance head drops sharply, i.e., the actuator assembly above the impedance head is resonating while producing negligible longitudinal motion between the impedance head and buffer material where the force is measured. The slight difference between the frequencies for the first configuration and the second two configurations suggest that the mass of the surrogate also affects the antiresonance. The resonance near 10,000 Hz follows a similar pattern to the resonance near 500 Hz, suggesting this resonance is associated with the actuator as well.

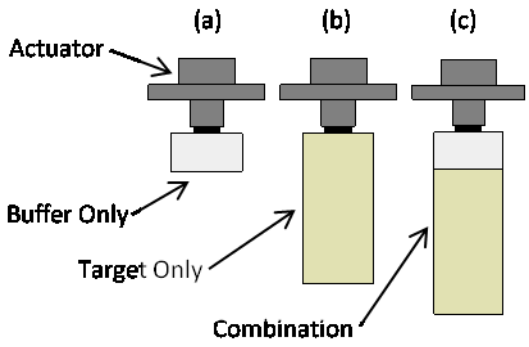

FIGURE 2: EXPERIMENTAL CONFIGURATIONS TESTED WITH (a) POLYCARBONATE BUFFER, (b) COMPOSITE TARGET, AND (c) COMPLETE STRUCTURE.

The physical properties and connectivity of the components of the test specimen were identified in order to develop a model to shed light on these experimental observations. The actuator (mass m_a=36.5 g and diameter D_a=5.08 cm) was stud mounted to the impedance head (mass m_h=24.2 g and mass moment of inertia I_h=3.81e-4 g·m^2 about the lateral axis), and then the impedance head was stud mounted to a washer, which was glued to the polycarbonate specimen (mass of m_b=7.7 g and mass moment of inertia I_b=3.10e-4 g·m^2) A proof mass (m_p=100.8 g and mass moment of inertia I_p=41e-4 g·m^2) was stud mounted to the opposite side of the actuator to increase the actuator force level. The (thickness, diameter) of the proof mass, impedance head, and polycarbonate specimen were (1.27 cm, 2.54 cm), (1.58 cm, 1.58 cm), and (1.27 cm, 2.54 cm), respectively. The test specimen was supported on a foam block with stiffness k_b and viscous damping c_b and the actuator possesses longitudinal stiffness k_a. These parameters are subsequently estimated.

The schematic in Figure 4(a) portrays the longitudinal and rotational dynamics of the actuator assembly, which is assumed to contain an imbalance, e, which causes the force across the actuator to produce a moment of reaction M_a. The corresponding free body diagrams are shown in Figure 4(b) including the polycarbonate cylinder. In both of these figures, a portion of the actuator mass and inertia is incorporated into the proof mass and impedance head.

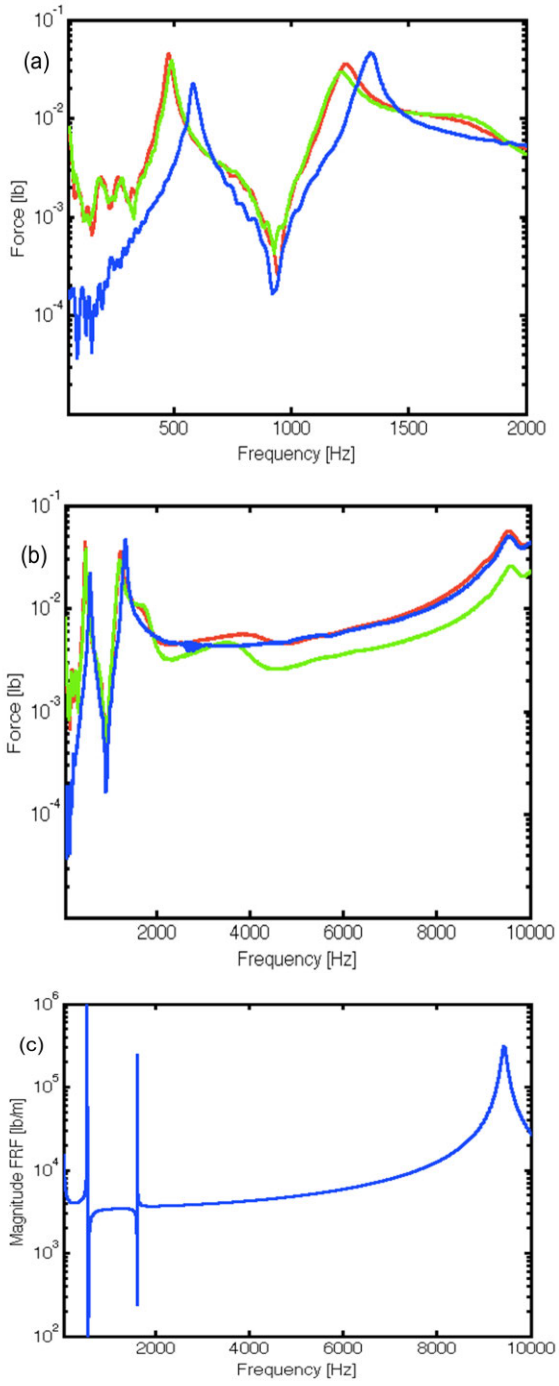

FIGURE 3: FORCE SPECTRA FOR THREE TEST CONFIGURATIONS, BUFFER (BLUE), TARGET (GREEN) AND COMPLETE STRUCTURE (RED) IN THE RANGE (a) 50-2,000 Hz, and (b) 50-10,000 Hz; (c) THE FREQUENCY RESPONSE FUNCTION MODEL DEVELOPED FOR THE ACTUATOR ASSEMBLY SHOWING AGREEMENT WITH THE EXPERIMENTALLY-RECOVERED RESONANCE AND ANTIRESONANCE STRUCTURE.

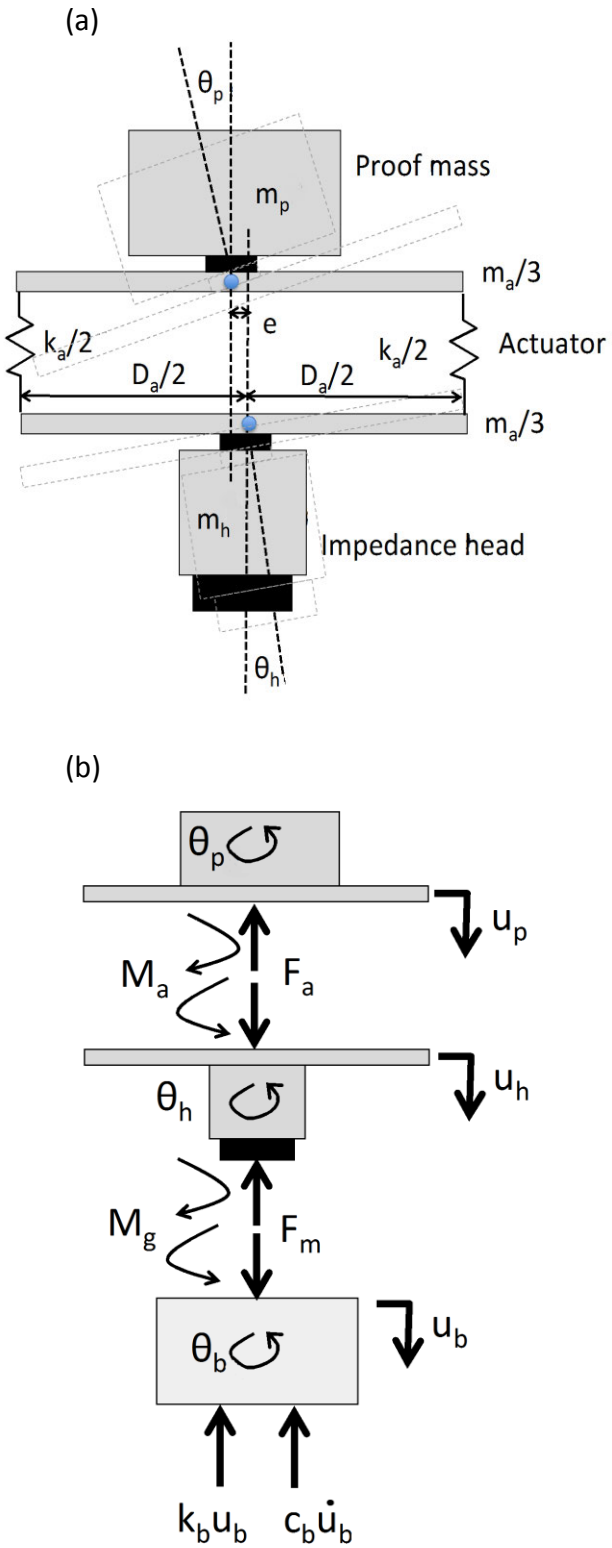

FIGURE 4: (a) SCHEMATIC OF ACTUATOR ASSEMBLY SHOWING MISALIGNMENT AND RESULTING COUPLING BETWEEN LONGITUDINAL AND ROTATIONAL MOTION. (b) CORRESPONDING FREE BODY DIAGRAM.

The corresponding equations of motion and kinematic constraints for Figure 4(b) are given below:

$$m'_p\ddot{u}_p = -F_a \tag{1}$$

$$I'_p\ddot{\theta}_p = -M_a \tag{2}$$

$$m'_h\ddot{u}_h = F_a - F_m \tag{3}$$

$$I'_h\ddot{\theta}_h = M_a - M_g \tag{4}$$

$$m_b\ddot{u}_b = F_m - k_b u_b - c_b\dot{u}_b \tag{5}$$

$$I_b\ddot{\theta}_b = M_g \tag{6}$$

$$F_a = k_a(u_p - u_h) - k_a e\theta_p \tag{7}$$

$$M_a = \frac{k_a}{2}\left[2e(u_h - u_p) + \left(\frac{D_a^2}{2} + 2e^2\right)\theta_p - \frac{D_a^2}{2}\theta_h\right] \tag{8}$$

$$F_m = k_g(u_h - u_b) \tag{9}$$

$$M_g = k_{tg}(\theta_h - \theta_b) \tag{10}$$

$$\Delta = u_p - u_h \tag{11}$$

where F_m is the measured force at the impedance head, F_a is the input force at the actuator, M_a and M_g denote the moment reactions across the actuator and glue beneath the impedance head, respectively, and $m'_p = m_p + m_a/3$ and $m'_h = m_h + m_a/3$ denote the modified mass values for the proof mass and impedance head mass when one-third of the actuator mass is added to each, $I'_p = \frac{1}{4}m_p\frac{D_p^2}{4} + \frac{1}{4}\frac{m_a}{10}\frac{D_a^2}{4}$ and $I'_h = \frac{1}{4}m_h\frac{D_h^2}{4} + \frac{1}{4}\frac{m_a}{10}\frac{D_a^2}{4}$ are the modified mass moments of inertia of the proof mass and impedance head when the contributions of the actuator are incorporated, and $I_b = \frac{1}{4}m_b\frac{D_b^2}{4}$. The stiffness of each stud in the assembly was assumed to be infinite in this model and the glue was assumed to have finite linear and torsional stiffness, k_g and k_{gt}. It was also assumed that the thicknesses of the proof mass and impedance head were negligible when computing moments.

By solving these equations simultaneously using Laplace transform techniques, the transfer function relating the actuator input, i.e., the relative motion across the actuator, to the measured force from the impedance head are found to be:

$$\frac{F_m(s)}{\Delta(s)} = k_a A(s)\left(1 + \frac{E(s)}{B(s)}\right) \tag{12a}$$

where

$$A(s) = \frac{k_g(m_b s^2 + c_b s^2 + k_b)}{m_h' m_b s^4 + m_h' c_b s^3 + [m_h'(k_b + k_g) + m_b k_g] s^2 + c_b k_g s + k_b k_g} \quad (12b)$$

$$B(s) = I_p' I_b I_h' s^4 + \left[I_b I_h' \left(e^2 + \frac{d_a^2}{4} \right) k_a + \frac{k_a d_a^2}{4} I_p' I_b + k_{tg} I_p' (I_h' + I_b) \right] s^2 + \frac{k_a k_{tg} d_a^2 I_p'}{4} + k_{tg} (I_h' + I_b) \left(e^2 + \frac{d_a^2}{4} \right) k_a \quad (12c)$$

$$E(s) = k_a e^2 [I_b I_h' s^2 + k_{tg} (I_h' + I_b)] \quad (12d)$$

The denominator of A(s) indicates there are two resonances due to the foam boundary condition and the glue underneath the impedance head, and the numerator indicates there is an antiresonance due to the foam. B(s) and E(s) indicate there are resonances and antiresonances due to the rotational dynamics of the actuator.

The stiffness and damping parameters in the transfer functions in equation (12) must be estimated. The strategy that was used to estimate these unknown parameters was to assume zero damping initially to estimate the stiffness coefficients. The stiffness of the foam was measured by applying a known weight and measuring the static deflection, resulting in a stiffness estimate of k_b=1,859 N/m. For the first of the three configurations shown in Figure 2, the experimental frequency spectrum for the measured force was then used together with Matlab® to iterate on the values of k_g, k_{tg}, and k_a. It was found that k_g largely dictates the location of the resonance slightly below 10,000 Hz, k_{tg} largely dictates the location of the third resonance, and k_a largely dictates the location of the second resonance, as well as the spread between the second and third resonances. e dictates the magnitude of the second two resonances. The values selected for these parameters were k_g=22e6 N/m, k_{tg}=78 N/m, k_a=20,000 N/m and e=5 mm. The resulting frequency response function magnitude that was produced using these parameters is plotted in Figure 3(c), which reflects the resonance and antiresonance structure of the experimental data in Figure 3(b).

BUFFER AND TARGET DYNAMICS

The analysis in the previous section indicates that frequencies below 2,500 Hz are strongly influenced by the actuator dynamics and that these dynamics involve both longitudinal and transverse motions. With this in mind, the velocity frequency response functions were measured in the longitudinal, transverse, and lateral directions at sixty-three points along the side of the polycarbonate and surrogate cylinders (see Figure 5) using a Polytec three-dimensional vibrometer. Figure 6 depicts the obtained velocity responses in the longitudinal and transverse directions for the 50% volume fraction (___) and 75% volume fraction (.) particulate composite samples. Note that the polycarbonate material was the same in both tests, and that vacuum grease was used at the interface of the two cylinders in each test. In addition, note that the plots in Figure 6(a-c) correspond to the points 3, 24, and 45, which are located above the interface in the polycarbonate (buffer) material and the plots in Figure 6(d-f) correspond to the points 4, 25, and 46, which are located beneath the interface in the composite (target) material

.

As the plots indicate, there are significant differences in the responses of the buffer material (solid and dashed blue lines) for the two different composite materials (50% and 75% volume fraction). For example, Figure 6(a) indicates that two of the resonant frequencies of the system shift from 920 to 1,240 Hz and 1,420 to 1,920 Hz, respectively. This shift in resonant frequency represents a 35% change, which is indicative of a change in modulus of the target material because the mass of the two specimens is nearly the same (39.6 g and 41.3 g). Assuming a longitudinal or bending mode of vibration, a 1.35× change is equivalent to an 82% increase in modulus, which reflects the greater volume fraction of crystals in the binder.

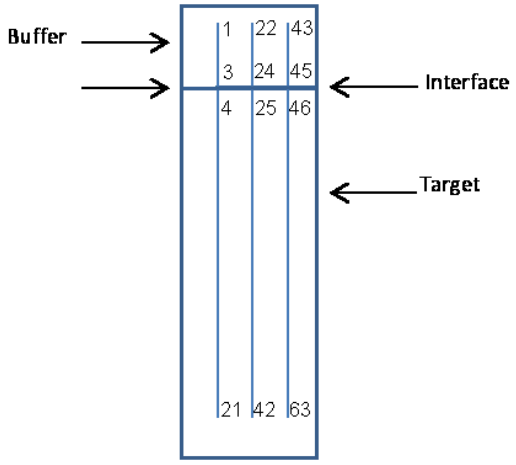

FIGURE 5: MEASUREMENT POINTS ALONG SIDE OF BUFFER AND TARGET CYLINDERS.

The plots in Figure 6(d-f) indicate that there are significant differences in the transverse direction responses above and below the interface (solid and dashed lines), whereas the differences in the longitudinal measurements across the interface (Figure 6(a-c)) are much less. This result

suggests that the longitudinal motions between the two bodies are more tightly coupled, perhaps leading to a more straightforward diagnostic measurement for the target material. In addition, note that the more compliant 50% vf target composite material generally exhibits a greater degree of coupling to the buffer material than the stiffer 75% vf material.

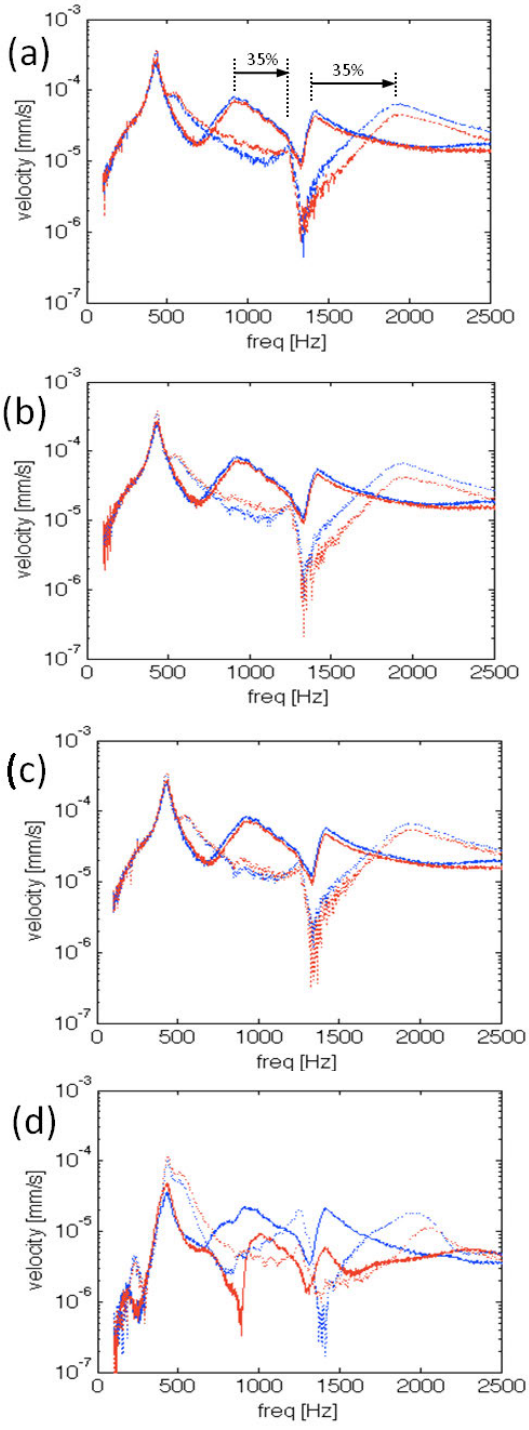

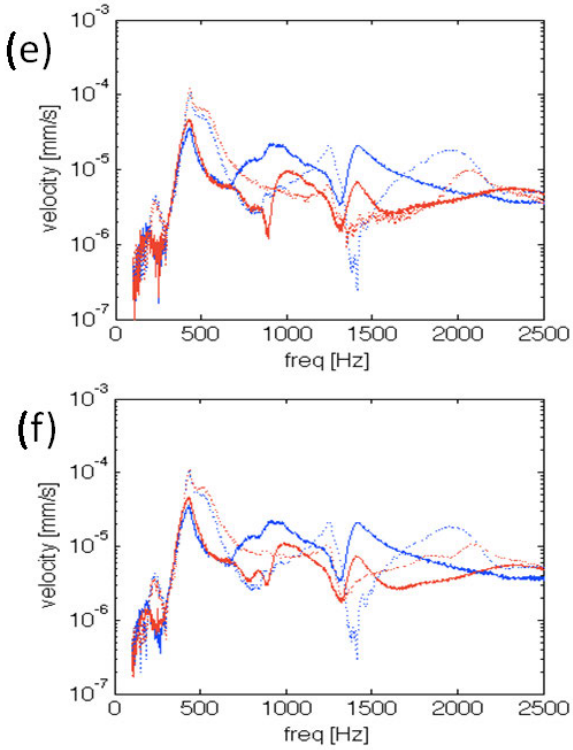

FIGURE 6: (a-c) LONGITUDINAL VELOCITY RESPONSE ON THE BUFFER MATERIAL (BLUE) AT POINTS 3, 24, AND 45, WHICH ARE LOCATED ABOVE THE INTERFACE, AND THE TARGET MATERIAL (RED) AT POINTS 4, 25, AND 46, WHICH ARE LOCATED BENEATH THE INTERFACE. (d-f) CORRESPONDING TRANSVERSE VELOCITY RESPONSES. 50% vf (___) and 75% vf (.).

The Complex Mode Indicator Function (CMIF) method was used to estimate the modal deflection shapes of the specimen by performing a singular value decomposition of the frequency response function matrix. Frequencies of interest include 430, 920 and 1,420 Hz in the 50% vf material and 430, 1,240 and 1,900 Hz in the 75% vf material. Figures 7(a-f) show plots of the modal deflection shapes at these frequencies that were extracted using the CMIF method. The mode shapes involve longitudinal, lateral, and transverse motions of the buffer and target. Note that the actuator dynamics are the source of the observed bending motions, which would otherwise not exist if the actuator were delivering only a longitudinal forcing function. The main difference between the two mode shapes is near the interface – there is much more separation between the buffer and target for the transverse motions observed in Figure 7 as was noted in Figure 6.

To identify any nonlinear vibration characteristics in the measured responses, tests were run at different amplitudes of excitation. The resulting velocity responses were then normalized to the lowest amplitude and plotted in Figure 8. Due to the larger amplitude relative motions between the buffer and target in the transverse direction, the nonlinearity is

most evident in this direction, particularly in the target material (red line) as highlighted in the figure.

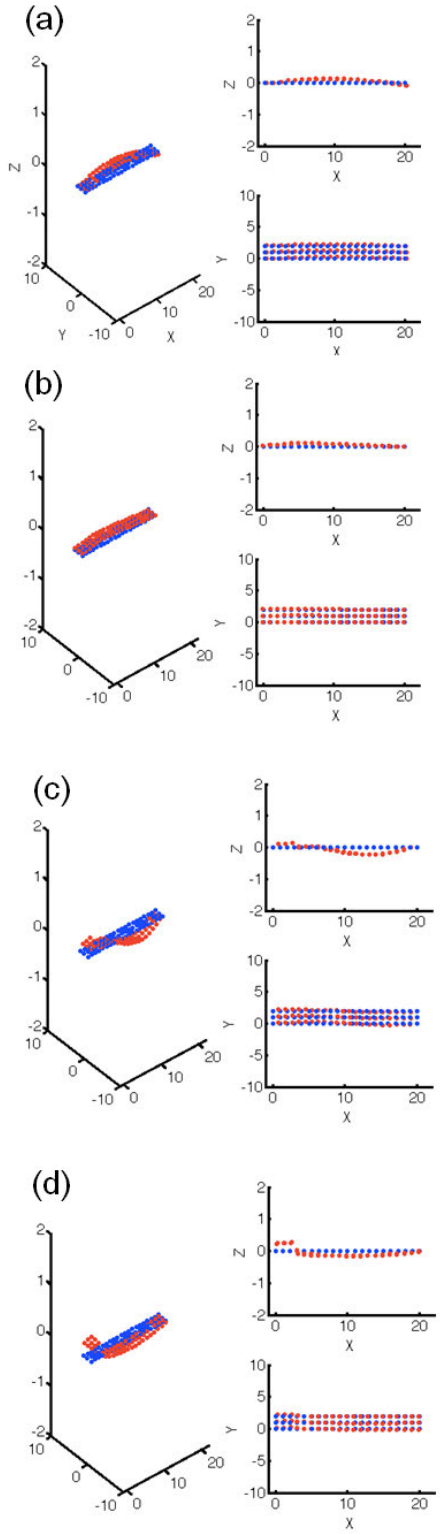

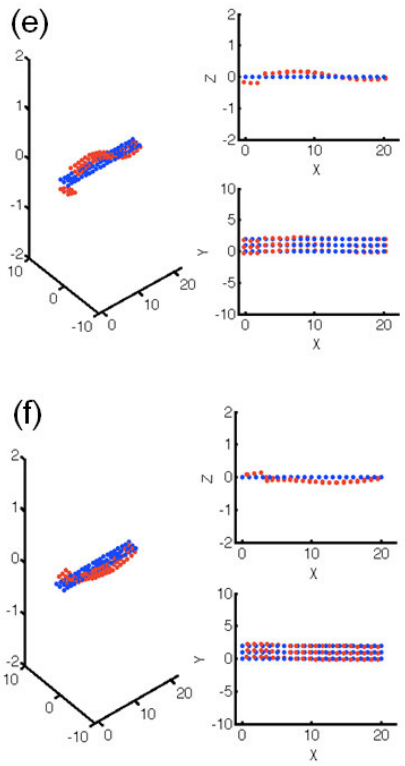

FIGURE 7: MODAL DEFLECTION SHAPES OF THE TWO-BODY SPECIMEN WITH SEVERAL VIEWS OF THE THREE COMPONENTS OF MOTION FOR (a) 435 HZ (50% vf), (b) 435 HZ (75% vf), (c) 920 HZ (50% vf), (d) 1,240 HZ (75% vf), (e) 1,420 HZ (50% vf) and (f) 2,000 HZ (75% vf). NOTE THAT BLUE IS USED TO DESIGNATE THE UNDEFORMED SHAPE.

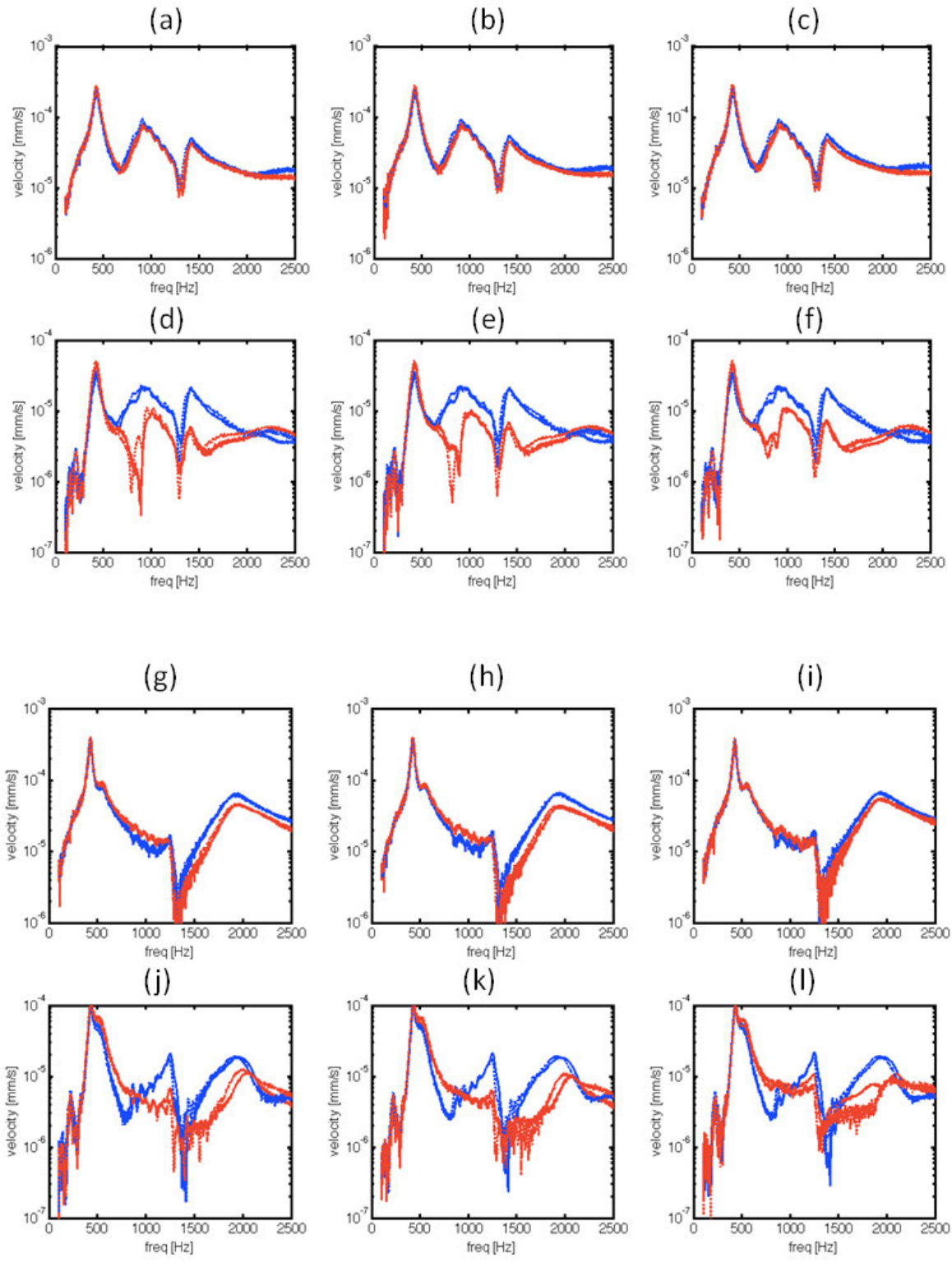

FIGURE 8: NORMALIZED VELOCITY RESPONSE FOR LOW (___) AND HIGH (.) AMPLITUDE FORCE WITH (a-f) 50% vf TARGET SAMPLE: (a-c) LONGITUDINAL AND (d-f) TRANSVERSE MEASUREMENTS; AND (g-l) 75% vf TARGET SAMPLE WITH (g-i) LONGITUDINAL AND (j-l) TRANSVERSE MEASUREMENTS.

CONCLUSIONS

Vibration measurements on a buffer material (polycarbonate) are used in this paper to characterize the properties of a target material (polymer particulate composite), which is located beneath the buffer. A three-dimensional laser vibrometer and piezoelectric inertial actuator are used to measure the broadband response. A transfer function model of the actuator is developed and it is shown that asymmetry in the actuator assembly produces both longitudinal and torsional excitations that are applied to the specimen. The change in modulus due to an increase in volume fraction of crystals is shown to cause a 35% shift in resonant frequencies, which display both longitudinal and transverse vibrations based on the Complex Mode Indicator Function analysis of the modal deflection shapes. It is also shown that the interface between the bodies causes the two bodies to decouple to a large degree above 1500 Hz. The larger volume fraction of crystals in the material also leads to more nonlinearity (due to increased stiffness) across the interface, especially in the transverse direction.

ACKNOWLEDGEMENTS

This research is supported by the U.S. Office of Naval Research under the Multidisciplinary University Research Initiative on "Sound and Electromagnetic Interacting Waves" through grant No. N00014-10-1-0958. The authors wish to acknowledge Jelena Paripovic and Prof. Patricia Davies for their efforts with regard to material property identification.

REFERENCES

Adams, R., Drinkwater, B., 1997, "Nondestructive Testing of Adhesively-Bonded Joints," NDT & E International, **30**(2), pp. 93-98.

Bertoldi, K., Bigoni, D., Drugan, W., 2007, "Structural Interfaces in Linear Elasticity. Part I: Nonlocality and Gradient Approximations," Journal of the Mechanics and Physics of Solids, **55**(1), pp. 1-34.

Bigoni, D., Movchan, A., 2002, "Statics and Dynamics of Structural Interfaces in Elasticity," International Journal of Solids and Structures, **39**(19), pp. 4843-4865.

Castellini, P., Revel, G., 2000, "Laser Vibration Measurements and Data Processing for Structural Diagnostics on Composite Material," Review of Scientific Instruments, **71**(1), pp. 207- 215.

Cerniglia, D., Djordjevic, B., Nigrelli, V., 2001, "Quantitative Subsurface Defect Detection in Composite Materials Using a Non-Contact Ultrasonic System," 2001 *IEEE Ultrasonic Symposium*, pp. 751-754.

Doebling, S., Farrar, C., Prime, M., 1998, "A Summary Review of Vibration-Based Damage Identification Methods," The Shock and Vibration Digest, **30**(2), pp. 91-105.

Donskoy, D., Sutin, A., Ekimov, A., 2001, "Nonlinear Acoustic Interaction on Contact Interfaces and Its Use for Nondestructive Testing," NDT & E International, **34**(4), pp. 231-238.

Guo, X., Zhang, D., Wu, J., 2010, "Quantitative Evaluation of Contact Stiffness between Pressed Solid Surfaces Using Dual-Frequency Ultrasound," Journal of Applied Physics, **108**(3), p. 034902.

Mang, J., Hjelm, R., Skidmore, C., Howe, P., 1996, "Parameterization of Structures in HE Composites using Surrogate Materials: A Small Angle Neutron Scattering Investigation," LA-UR-96-2087, US Dept of Defense.

Montalvao, D., Maia, N., Ribeiro, A., 2006, "A Review of Vibration-based Structural Health Monitoring with Special Emphasis on Composite Materials," The Shock and Vibration Digest, **38**(4), pp. 295-324.